Assessing the impact of seasonal rainfall anomalies on catchment-scale water balance components

Paolo Nasta[1,*], Carolina Allocca[1], Roberto Deidda[2], Nunzio Romano[1,3]

[1] Department of Agricultural Sciences, AFBE Division, University of Naples Federico II, Portici (Napoli), Italy.

[2] Department of Civil and Environmental Engineering and Architecture, University of Cagliari, Cagliari, Italy.

[3] The Interdepartmental Research Center for Environment (C.I.R.AM.), University of Naples Federico II, Napoli, Italy.

Correspondence to: Paolo Nasta (paolo.nasta@unina.it)

Keywords: Mediterranean climate, Budyko curve, drought, Standardized Precipitation Index, SWAT model, Upper Alento River Catchment

Abstract. Although water balance components at the catchment scale are strongly related to annual rainfall, availability of water resources in Mediterranean catchments also depends on rainfall seasonality. Observed seasonal anomalies in historical records are fairly episodic, but an increase in their frequency might exacerbate water deficit or water excess if the rainy season shortens or extends its duration, e.g. due to climate change. This study evaluates the sensitivity of water yield, evapotranspiration, and groundwater recharge to changes in rainfall seasonality by using the Soil Water Assessment Tool (SWAT) model applied to the Upper Alento River Catchment (UARC) in southern Italy where a long time series of daily rainfall is available from 1920 to 2018. We compare two distinct approaches: *i*) a "static" approach, where three seasonal features (namely rainy, dry, and transition fixed-duration 4-month seasons) are identified through the standardized precipitation index (SPI); *ii*) a "dynamic" approach based on a stochastic framework where the duration of two seasons (rainy and dry seasons) varies from year to year according to a probability distribution. Seasonal anomalies occur when the transition season is replaced by the rainy or dry season in the first approach and when season duration occurs in the tails of its normal distribution in the second approach. Results are presented within a probabilistic framework. We also show that the Budyko curve is sensitive to the rainfall seasonality regime in UARC by questioning the implicit assumption of a temporal steady state between annual average dryness and the evaporative index. Although the duration of the rainy season does not exert a major control on water balance, we were able to identify season-dependent regression equations linking water yield to the dryness index in the rainy season.

1. **Introduction**

The rainfall regime of the Mediterranean climate is characterized by the alternation of wet and dry periods within the year, with evident out-of-phase seasonal behavior of precipitation and temperature patterns. Most annual rainfall is concentrated in the late fall, winter, and early spring, while late spring, summer, and early fall are usually hot and quite dry. Rainfall seasonality plays a fundamental role in planning and managing water resources in countries subject to a Mediterranean climate. Summer is characterized by water stress due to scarce rainfall supply, combined with high evapotranspiration loss and the seasonal peak in water consumption (comprising agricultural, industrial, and recreational uses, hydroelectric power generation, as well as domestic uses, which are often boosted by tourism pressure). Therefore, it is necessary to store water during the rainy period to cope with the uncertain duration of adverse water deficit conditions during the dry period. Water-supply infrastructures necessitate high investment costs that strongly depend on the expected balance between the amount of water supplied in the rainy period and the amount of water lost and consumed during the dry season. The amount of rainfall in each season can be suitably decomposed and simulated on the basis of the following three main components: *i*) duration of the seasons; *ii*) occurrence probability of a daily rainfall event in each season; *iii*) mean depth of daily rainfall events in each season (Van Loon et al., 2014). A combination of the last two factors determines the rainfall magnitude in each season (Feng et al., 2013).

A very small or very large amount of water (exceeding a certain threshold value for a specified return period and duration) supplied in each season can be interpreted as a seasonal precipitation anomaly and is usually observed episodically in a historical multi-decadal time-series of annual rainfall values. Seasonal precipitation anomalies result mainly from a combination of the duration of the wet season and its rainfall magnitude. These two factors should be taken into due account when planning water-supply infrastructures (Apurv et al., 2017). The most recent reports released by the Intergovernmental Panel on Climate Change (IPCC) warn of the projected increase in seasonal anomalies induced by global warming in the Mediterranean region, with a considerable decrease in annual precipitation

52 and warming-enhanced evapotranspiration associated with rather severe and prolonged droughts, as recently observed

53 in southern Europe in 2003, 2015, and 2017 (Mariotti et al., 2008; Laaha et al., 2017; Hanel et al., 2018).

54 Studies underway in the Upper Alento River Catchment (UARC) in southern Italy offer a good chance to understand

55 the effects of seasonal rainfall uncertainty on water supply generation given the presence of a multi-purpose earthen

56 dam (known as Piano della Rocca) constructed to regulate water for irrigation, hydropower generation, flood control,

57 and drinking purposes. The main research question, also raised or prioritized in some way by local stakeholders in their

58 decision-making processes, can be expressed as follows: "*What is the impact of seasonal rainfall anomalies on annual*

59 *average (or seasonal average) water supply in UARC?*". This question is particularly relevant to hilly catchments

60 similar to UARC within the Mediterranean region such that UARC could become a pilot area for dealing with some

61 specific problems and carrying out paired-catchment analyses.

62 This study therefore aimed to quantify the effects exerted by seasonal rainfall anomalies on water balance components.

63 With a view to coordinating interaction with stakeholders, end-users, and professionals, we performed this task by

64 implementing the well-known and well-validated Soil Water Assessment Tool (SWAT) model (Arnold et al., 1998).

65 Particular attention is devoted to computing water yield supplying the artificial reservoir bounded by the Piano della

66 Rocca earthen dam in ARC (Romano et al., 2018). One of the strengths of our approach lies in the availability of long-

67 term rainfall time-series (about a century of daily data) and detailed soil and land cover maps, enabling reliable

68 catchment-scale model simulations. Reliable scenario-based projections are built to investigate whether the longer-than-

69 average duration of the wet season implies a higher-than-average mean annual rainfall and consequently higher-than-

70 average water yield. To investigate this issue, our research strategy couples the seasonal duration with daily rainfall

71 occurrences and depths by using a Monte Carlo approach to obtain SWAT-simulated water balance components within

72 a general probabilistic framework.

Many authors have attempted to quantify rainfall seasonality using different approaches (Ayoade, 1970; Markham 1970; Nieuwolt, 1974; Oliver, 1980; Walsh and Lawler, 1981; Zhang and Qian, 2003; Martin-Vide, 2004; Potter et al., 2005; Feng et al., 2013; de Lavenne and Andréassian, 2018). The precipitation concentration index (PCI) proposed by Oliver (1980) is the most popular approach for quantifying the year-round precipitation distribution in a given study area (Raziei, 2018). Sumner et al. (2001) analyzed the spatial and temporal variation of precipitation seasonality over eastern and southern Spain by using the seasonality index (SI). The SI was also utilized to examine the spatial and temporal variability of precipitation seasonality in Greece (Livada and Asimakopoulos 2005), USA (Pryor and Schoof 2008), and northern Bangladesh (Bari et al. 2016). Under the typical Mediterranean climate of Sardinia (Italy), Corona et al. (2018) used the SI to evaluate the role of precipitation seasonality on runoff generation. Nonetheless, while PCI and SI are useful indexes to classify rainfall seasonality and the degree of concentration of rainfall within the year, their implementation in a Monte Carlo framework is not straightforward. Therefore, we opted to characterize rainfall seasonality and its anomalies by using the two approaches described as follows. A first approach, which is hereafter referred to as the static approach, is based on the analysis of the standardized precipitation index (SPI) to define the duration of a wet season (4 months), a dry season (4 months) and a transition season (2 months from dry to wet phase plus 2 months from wet to dry phase) in UARC. In this approach, the drought anomaly is rigidly built with the artifact of extending the duration of the dry season to eight months by removing the transition season. The same criterion applies to a prolonged duration of the rainy season. The second approach, instead, exploits the seasonality characterization proposed by Feng et al. (2013) and can be viewed as a dynamic approach since the duration of the rainy season is time-variant (inter-annual variability) and can be stochastically generated with random duration values drawn from their statistical distribution. This second approach investigates what happens to the water budget if the duration of the rainy season becomes shorter-than-normal (i.e. rainfall scarcity) or longer-than-normal (i.e. rainfall excess). As far as we are aware, there is still a lack of knowledge about the effects of possible changes in rainfall seasonality on the water balance of a catchment subject to a Mediterranean climate, and the analyses presented in this paper aim primarily to contribute to fill this gap.

2. Study area and experimental analyses

The Upper Alento River Catchment (UARC) is situated in the Southern Apennines (Province of Salerno, Campania, southern Italy) and has a total drainage area of about 102 km^2 (Fig.1). The Piano della Rocca dam is an earthen embankment with an impervious core that has been operating since 1995. The area consists mostly of relatively poor-permeable arenaceous-clayey deposits and secondarily of arenaceous-marly-clayey and calcareous-clayey deposits (Romano et al., 2018).

Please insert Fig. 1 here

A weather station managed by the Italian Hydrological Service is located near the village of Gioi Cilento and provides a dataset of daily rainfall values covering the period 1920-2018 (about 90 years), with an interruption of nine years (1942-1950) straddling World War II (Nasta et al., 2017). The data set of annual rainfall sums derived from the daily rainfall time series has a mean of 1,229.3 mm, while other metrics (median, standard deviation and coefficient of variation) are reported in the last row of Table 1. The same statistics are also summarized for rainfall depths in each month of the year. The variability exhibited by the monthly time series of rainfall depths is also depicted in Figure 2, denoting a typical Mediterranean seasonal cycle. A large amount of precipitation occurs in the months from October to March, a period commonly identified as a wet period of the hydrological year, and accounts for about 68% of the annual mean rainfall (i.e. 834.9 mm over 1,229.3 mm) (see Table 1 and Figure 2). November is the wettest month with an average monthly rainfall of 166.9 mm (about 14% of mean annual rainfall). In contrast, lower mean monthly rainfall depths are concentrated from April to September, which commonly identify a dry period of the hydrological year, with a cumulative rainfall over this period of 394.5 mm with respect to the annual mean of 1,229.3 mm, hence representing about 32% of mean annual rainfall. July is the driest month with a monthly mean rainfall of 29.8 mm (i.e. 2% of mean annual rainfall).

Please insert Fig. 2 here

Please insert Table 1 here

120   Within the monitoring activities of the MOSAICUS (MOnitoring and modeling Soil–vegetation–atmosphere processes

121   in the Alento river basin for Implementing adaptation strategies to Climate and land USe changes) project (Nasta et al.,

122   2013; Romano et al., 2018), an automated weather station was installed in 2004 close to the village of Monteforte

123   Cilento and equipped with sensors for monitoring rainfall, wind speed and direction, air temperature and relative

124   humidity, and solar radiation, to record such meteorological variables at 15 min intervals (Nasta et al., 2019). The

125   statistical distributions of weather data recorded at the weather station of Monteforte Cilento (2004-2018) will be used

126   to calculate potential evapotranspiration as described in Section 3.

127   In this study, we used the most recent available land-use map drawn up in 2015 by using second-level CORINE

128   (Coordination of Information on the Environment) Land-Cover classes (CORINE 2006 land cover dataset;

129   http://www.eea.europa.eu): forest, arable land (annual crops), permanent crops (orchards, vineyards, olive groves, and

130   fruit trees), pasture, urban fabric, and water bodies. Forest (evergreen and deciduous trees, and multi-stem evergreen

131   sclerophyllous Mediterranean shrubs) and agricultural (arable land, permanent crops, and orchards) cover about 70%

132   and 20% of the catchment, respectively (Nasta et al., 2017). A five-meter resolution Digital Terrain Model (DTM) was

133   used to generate the hydrographic network and a soil-landscape units map is used to depict soil attributes in UARC

134   (Nasta et al., 2018).

3. Parameterization of the SWAT Model

136   The Soil Water Assessment Tool (SWAT) is a bucket-type, semi-distributed hydrological model operating on a daily

137   time scale and at a catchment spatial scale (Arnold et al., 1998). The main components of the water balance equation are

138   the daily change in water storage (ΔWS) as affected by rainfall (R), actual evapotranspiration (ET_a), groundwater

139   recharge (GR), and water yield (WY). Water yield is given by the contribution of surface runoff, groundwater

140   circulation, and lateral flow within the soil profile, and is partially depleted by transmission losses from tributary

141   channels and water abstractions. All variables are expressed in units of mm of water height.

142   SWAT requires as input rainfall (R) and potential evapotranspiration (ET_p) time series at a daily scale and is based on

143   the concept of hydrological response units (HRUs), which are areas identified by similarities in soil, land cover, and

144   topographic features, where hydrological processes are represented by a lumped schematization. The five-meter DTM

145   of the study area was used to determine the catchment boundaries, the hydrographic network, and thirteen distinct

146   HRUs. Catchment-lumped parameters are assigned to each HRU through look-up tables. By using the available soil-

147   landscape unit map, the input parameters were assigned according to the model set-up as presented in Nasta et al.

148   (2017). Nine parameters were calibrated to achieve the best model fit between simulated and measured monthly water

149   yield data recorded from 1995 and 2004 (Nasta et al., 2017). Such hydrological parameters include the soil evaporation

150   and compensation factor, plant uptake compensation factor, Manning's value for overland flow, the baseflow recession

151   constant (groundwater flow response to changes in recharge), groundwater delay time, groundwater "revap" coefficient

152   (controlling water that moves from the shallow aquifer into the unsaturated zone), Manning's coefficient for the main

153   channel, effective hydraulic condition in the main channel alluvium, and the bank storage recession curve. Model

154   performance proved to be satisfactory at a monthly time scale. We ran numerical simulations at a daily time step

155   (rainfall was randomly generated at a daily time step) and aggregated the output fluxes at a monthly time resolution.

156   Although there is evidence in the body of scientific literature of a potential misfit between measured and simulated

157   water yield values at a daily time-scale when calibrating a model with data at a monthly time resolution (Adla et al.,

158   2019), we are confident that our results and conclusions will not be affected by this drawback. Our analysis is based on

159   the monthly aggregation of fluxes and is aimed at analyzing seasonal patterns of monthly aggregates.

160   This study is based on modeling scenarios implemented in SWAT through a Monte Carlo approach, where each

161   simulation is three years long. Results from the first two-year warm-up period are discarded, while water balance

162   components simulated for the third year are stored for subsequent analysis. Initial soil water storage is set as field

163   capacity. The model simulations of the first two years are disregarded in order to erase the impact of the initial

164   (unknown) soil moisture values set in the soil domain. We point out that initial soil water content set at field capacity

165   can be considered a realistic situation in winter under the Mediterranean climate. The rainfall data are generated for the

166   static and dynamic approaches (described below) using a probability setting calibrated on daily rainfall values recorded

167   at the Gioi Cilento weather station (1920-2018). Mean and standard deviation of the meteorological data (wind speed,

168   air temperature and relative humidity, and solar radiation) recorded at the second automated weather station (close to

169   the village of Monteforte Cilento) are calculated each month. Daily potential evapotranspiration data were calculated by

170   using random values of weather data drawn from their normal distribution in each month of the year (Allen et al., 1998).

171   Results were provided as input to SWAT to randomly generate daily potential evapotranspiration by using the Penman-

172   Monteith equation (Allen et al., 1998).

173   **4. Determination of rainfall seasonality**

174   **4.1. Static approach based on the SPI drought index**

175   The intra-annual rainfall regime under a Mediterranean climate can be characterized through the distribution of annual

176   rainfall depth among different seasons (Paz and Kutiel, 2003; Kutiel and Trigo, 2013). The seasonal pattern occurring in

177   the study area is here characterized by analyzing the distribution of the standardized precipitation index (SPI) on a long-

178   term monthly rainfall time series. The SPI is a probability index developed to classify rainfall anomalies and often

179   employed as an indicator of potential (meteorological) droughts over many time scales (McKee et al., 1993; Hayes et

180   al., 1999). Computation of the SPI should rely on long-term rainfall datasets (e.g. 30 years, according to climatological

181   standards), and is usually obtained by projecting a Gamma distribution fitted on rainfall depths cumulated on 1, 3, 6, 12,

182   18, or 24 months (referred to as SPI-1, SPI-3, SPI-6, SPI-12, SPI-18, or SPI-24, respectively) into a standardized normal

183   distribution. The short-term SPI (e.g. 3-month time scale) can provide useful information for crop production and soil

184   moisture supply, while the long-term SPI (e.g. 12- or 24-month time scale) can give insights on water availability for

185   groundwater recharge. Negative SPI values indicate drier-than-expected rainfall, whereas positive SPI values refer to

186   wetter-than-expected months. To quantify the degree of departure from median conditions, McKee et al. (1993)

187   proposed a rainfall regime classification. Since the SPI is given in units of standard deviation from the standardized

mean, this statistical index enables also the precipitation anomaly to be identified through the magnitude of its value: values ranging from −0.99 to +0.99 are considered near normal, from +1.00 to +1.49 (or from −1.49 to −1.00) indicate moderately wet (or moderately dry) periods, from +1.50 to +1.99 (or from −1.99 to −1.50) very wet (or very dry) periods, and above +2.00 (or below −2.00) extremely wet (or extremely dry) periods. Therefore, the extent of SPI departure from the mean (i.e. from the zero value) gives a probabilistic measure of the severity of a wet (if positive) or dry (if negative) period. By exploiting the properties of the (standard) normal distribution, the probabilities of obtaining SPI values greater than +1, +2, and +3 (or less than −1, −2, and −3) are 15.90%, 2.28% and 0.14%, respectively.

To emphasize the seasonal cycle of intra-annual rainfall patterns within a probabilistic framework, we used the SPI-1 by fitting the Gamma distribution on all monthly rainfall depths, i.e. pooling observations from all months in each year. In such a way, the months characterized by SPI-1 values below, around or above the zero line can be assumed to belong to the dry, transition or wet seasons, respectively.

4.2. Dynamic approach based on the duration of the wet season proposed by Feng et al. (2013)

According to Feng et al. (2013), the dimensionless seasonality index (DSI) is based on the concept of relative entropy and quantifies the rainfall concentration occurring in the wet season. The DSI is zero when the average annual rainfall is uniformly distributed throughout the year and maximized at 3.585 when maximum average annual rainfall is concentrated in one single month (Pascale et al., 2016); see the Appendix for details. Feng et al. (2013) proposed to describe the rainfall seasonality through the following three components: annual rainfall depth (magnitude), centroid (timing), and spread (duration) of the wet season (see also Pascale et al., 2015; Sahani et al., 2018). As described in Section 5.2 and according to appropriate statistical tests, we found that a normal distribution can reasonably describe the 90 wet season durations obtained by applying to the observed rainfall time series the procedure proposed by Feng et al. (2013), and briefly summarized in the Appendix. Thus, each hydrological year will consist of the alternation of only two seasons: the wet season with a duration that is randomly generated by a normal distribution with mean and standard deviation estimated on the Gioi Cilento time series, and a dry season in the subsequent months of the year.

4.3 Set-up of Monte-Carlo rainfall scenarios in SWAT

Seasonal rainfall anomalies, although episodic, can affect the water balance components at the catchment scale. As suggested by Domínguez-Castro et al. (2019), the impact of such anomalies can be quantified within a probabilistic framework. For the Upper Alento River Catchment (UARC), we evaluated the effects of seasonal anomalies by running SWAT simulations with synthetic rainfall time series considering different hypotheses (scenarios) of alternations of seasons, according to the static and the dynamic approaches described above. In each season, we assumed that rainfall evolution in time can be represented by a stochastic Poisson point process of daily rainfall occurrences, with daily rainfall depth following a proper probability distribution (Eagleson, 1972; Rodríguez-Iturbe et al., 1987; Veneziano and Iacobellis, 2002). Synthetic rainfall time series were then generated, keeping constant parameters of the Poisson process and daily rainfall parent distribution in each season.

A preliminary analysis was conducted to investigate the best parent distribution for observed rainfall daily depths. With this aim, we used the L-moment ratios diagram proposed by Hosking (1990) (see also Vogel and Fennessey, 1993) as a diagnostic tool. Results are shown in Figure 3 where the L-skewness and L-kurtosis computed on the time series left-censored with a threshold of 3 mm (large filled circle) is compared with the theoretical expectation of the same L-moment ratios for several probability distributions commonly adopted in statistical hydrology. An ideal candidate as parent distribution seems the Generalized Pareto distribution (GPd), although it is also worth noting that sample estimation of L-skewness and L-kurtosis (0.3437, 0.1706) is very close to the expected values for exponential distribution (1/3, 1/6). As visual support for this preliminary analysis, the exponential probability plot in Figure 4 compares the empirical cumulative distribution function F(x) of the observed time series (circles) with the fitted GPd (dashed line) and the fitted exponential distribution (continuous line). The two models are very close to each other for the whole body of observation, with only a slight departure of the GPd from the straight line characterizing the exponential distribution due to a very slight right tail. This evidence gave us the confidence to adopt the single-parameter exponential model as parent distribution for series partitioned according to the seasons defined above, thereby reducing the uncertainty related to the additional shape parameter of the GPd. Finally, it is worthwhile

235 mentioning that both distributions shown in Figure 4 were fitted by applying Deidda's (2010) multiple-threshold-

236 method (MTM) on a range of thresholds from 2.5 to 12.5 mm to prevent biases due to very low records and data

237 discretization (Deidda, 2007). The MTM was then applied to estimate the exponential parameter η (mm) and the

238 probability occurrence of rainy days λ (d^{-1}) for each season considered.

239 For each scenario pertaining to either the static or dynamic approach, we generated 10,000 equi-probable realizations of

240 synthetic daily rainfall time series, each three years long, according to a stochastic Poisson point process model. In each

241 modeling scenario, the synthetic time series was then used as input for the SWAT model to evaluate the effects on the

242 water balance components in UARC. As anticipated in Section 3, the first two years represent warm-up simulations and

243 were thus discarded, while only results for the third year were stored for subsequent analyses presented in the next

244 section.

245 *Please insert Fig. 3 here*

246 *Please insert Fig. 4 here*

247 To further evaluate the hydrologic behavior of the study catchment, an issue deserving more detailed attention is the

248 assessment of the sensitivity of water balance to rainfall seasonality. With this aim, we refer to the Budyko framework

249 (Budyko, 1974), which has been extensively applied to relate water components in different climatic contexts

250 worldwide, including the Mediterranean climate (see e.g. Viola et al., 2017, Caracciolo et al. 2017). Specifically, the

251 Budyko framework relates the evaporative index (ET_a/R) to the dryness index (ET_p/R) computed at an annual time scale

252 in terms of "available water" (i.e., rainfall R). Potential evapotranspiration, ET_p, is limited by either energy supply (for

253 the dryness index less than or equal to one) or water supply (for the dryness index greater than one), and therefore the

254 Budyko space has two physical bounds dictated by either the atmospheric water demand ($ET_a \leq ET_p$) or the atmospheric

255 water supply ($ET_a \leq R$). The first bound is the energy limit (or demand limit, i.e. the 1:1 line corresponding to $ET_a = ET_p$)

256 implying that actual evapotranspiration cannot exceed potential evapotranspiration. The second bound is the water limit

257 (or supply limit, i.e. the horizontal line corresponding to $ET_a=R$) implying that actual evapotranspiration cannot exceed

258 precipitation when the dryness index is greater than one (i.e. $ET_p/R>1$).

259

5. Results and discussion

5.1. Static approach for assessing rainfall seasonality

262 The observed temporal evolution of SPI-6 in our 90-year time series (see gray bars in Fig. 5) highlights prolonged

263 droughts amongst the 1980s and 1990s and prolonged wet periods in the last decade when SPI-6 values above the

264 threshold +2 occurred in 2008, 2010, and 2012. Yet, by splitting the SPI-6 values into two 45-year sub-groups, we can

265 observe that the last 45-year period is characterized by a drier climate compared to the first 45-year period. Specifically,

266 in the first sub-group the probabilities of obtaining SPI-6>+1 and SPI-6<−1 are 17.9% and 7.6%, respectively. In

267 contrast, in the second sub-group there is a general increase in negative SPI-6 values: the probability of obtaining SPI-

268 6>+1 becomes 11.9% and that of obtaining SPI-6<−1 19.3%. By analyzing daily rainfall datasets recorded at 55

269 weather stations located in the region of Basilicata near UARC (characterized by similar climatic conditions), Piccarreta

270 et al. (2013) observed a general decreasing trend in the mean annual rainfall over the period 1951–2010 mainly due to

271 the autumn-winter decrease in precipitation.

272 *Please insert Fig. 5 here*

273 We now discuss the results pertaining to the calculation of the seasonal pattern of SPI-1 values. Rainfall seasonality

274 under a Mediterranean climate can be assumed to be roughly represented by the alternation of two six-month seasons,

275 characterized by positive and negative SPI-1 values (wet and dry season, respectively) (Rivoire et al., 2019). The

276 temporal evolution of the SPI-1 values is represented by the gray bars in Fig. 6a and highlights the seasonal cycle within

277 each year, whereas their 12-month moving average (magenta line in Fig. 6a) oscillates around the zero value with

278 prolonged dry periods during the 1980s and 1990s and prolonged wet periods in the 2000s and 2010s. Fig. 6b shows the

279 box and whiskers plots of the SPI-1 values for each month of the year, thus depicting the monthly distribution of this

280   index throughout the available recorded period. The median SPI-1 values (central red line in the blue boxes) are

281   negative only from May to August and positive from September to April, even though the whiskers (identified by the

282   two lines at the 25th and 75th percentile) denote the presence of relatively large variability in almost all months. Closer

283   inspection of this graph enables one to identify three main seasonal features: *i*) a dry period from May till August with

284   median values below zero; *ii*) a rainy period from November till February with median values above zero; *iii*) two

285   transition periods from wet to dry (March and April) and from dry to wet (September and October) with median values

286   near zero. We are aware that the median values in March, April, and October of the transition season are above zero,

287   rather than "near" zero, but we recall that the Mediterranean climate in UARC is sub-humid mainly due to orographic

288   influences. However, this approach is intrinsically a "static" procedure since the subdivision of the twelve months into

289   three groups is rigid even though months in the transition periods have high variability in SPI-1 values. This outcome

290   refines the initial working hypothesis of seasonal alternation of two semesters.

291   *Please insert Fig. 6 here*

292   The frequency distributions of the SPI-1 values computed over the rainy, dry, and transition seasons are illustrated in

293   Fig.6c-6d-6e. The wet season (depicted by the blue histograms) is characterized by probabilities of having SPI-1 values

294   greater than 0, +1, +2, and +3 of 80.60%, 30.50%, 1.90%, and 0.30%, respectively. The dry season (depicted by the red

295   histograms) is associated with SPI-1 values lower than 0, −1, −2, and −3 with probabilities of 78.10%, 31.10%, 0.56%

296   and 0.10%, respectively. Conversely, we warn that probabilities of obtaining positive SPI-1 values in the transition

297   season are 63.30% instead of the expected 50% if the hypothesis were "perfectly true". Therefore, we considered three

298   different scenarios, each with fixed and recurrent alternation of seasons during the hydrological year: *i*) a "reference

299   scenario" with a four-month wet season (NDJF), a four-month dry season (MJJA), and a four-month transition season

300   (MA from wet to dry and SO from dry to wet); *ii*) a "dry scenario", which mimics an extreme drought anomaly,

301   characterized by a prolonged eight-month dry season (from March to October) and abrupt alternations with the four-

302   month wet season (NDJF), without any transition season; *iii*) a "wet scenario", which mimics an extreme rainy

303   anomaly, characterized by a prolonged eight-month wet season (from September to April) and abrupt alternations with

304   the four-month dry season (MJJA), again with no transition season.

305   In light of the above results, the two Poisson parameters (η and λ) describing daily rainfall values were calculated for

306   each of the three seasons in the "reference scenario" and were then also used to develop synthetic simulations of rainfall

307   time series in the "dry" and "wet" scenarios (see Table 2).

308   *Please insert Table 2 here*

309

310   **5.2. Dynamic approach for assessing rainfall seasonality**

311   The centroid of the monthly rainfall distribution measured at the Gioi Cilento weather station (in the 90 years between

312   1920 and 2018) indicates that the wet season is centered in the second half of December, while its average duration is

313   about 5.44 months (see Fig. 7). Nonetheless, it is worth noting the occurrence of a few extreme situations: the severe

314   drought recorded in 1985 caused a minimum duration of about four months of the rainy period, while the year 1964

315   registered a maximum duration of about 7.0 months. The term "dynamic" used for this approach stems mainly from the

316   fact that the duration of the rainy period is time-variant throughout the years.

317   *Please insert Fig. 7 here*

318   The dimensionless seasonality index (DSI) and the seasonality index (SI) were computed for the Gioi Cilento time

319   series according to procedures proposed by Feng et al. (2013) and by Walsh and Lawler (1981), respectively. The

320   Mann-Kendall nonparametric test (Mann, 1945; Kendall, 1975) was then applied to evaluate possible decreasing,

321   increasing, or absence of temporal trends on these indexes, and revealed that the null hypothesis of absence of trend

322   cannot be neglected at the 0.05 significance level for both indexes. The stationarity in time of the DSI (red line) and SI

323   (green line) is also apparent from a perusal of Fig. 8, where the linear regressions (dashed and dotted for the DSI and SI,

324   respectively) are characterized by very weak downward slopes.

As described in Section 4.2, the dynamic approach assumes the alternation of only two seasons (wet and dry) with random durations of the rainy period. Figure 9a shows the time series of the 90 durations of the wet season estimated with the procedure proposed by Feng et al. (2013), while their frequency distribution is plotted in Fig. 9b. We then applied the Lilliefors statistical test (Lilliefors, 1967) to the null hypothesis of normality for the estimated wet durations obtaining a *p*-value of 0.327, meaning that the null hypothesis cannot be rejected with the commonly adopted 5% significance level. For each hydrological year, we thus generate a duration of the wet season from a normal distribution with the same mean and standard deviation of the Gioi Cilento time series (with a mean of 2.71 months and standard deviation of 0.28 months), while the dry seasons were consequently obtained as the complement in the same year to the wet seasons. In this case, the two Poisson parameters (η and λ) for modeling daily rainfall values were computed for the wet and dry seasons (Table 3).

5.3. Effects of seasonal rainfall anomalies on water balance when using the static approach

The results obtained from the three scenarios pertaining to the static approach are presented using the descriptive statistics of the water balance components at the annual time scale obtained from 10,000 SWAT simulation runs (Table 4). The reference scenario represents the normal situation with three seasons (dry, transition, and wet). Even though the range of annual rainfall values is relatively large, the coefficient of variation (CV) is only 14%, implying that very low and very high annual rainfall depths (outliers) occur occasionally. The water balance components, namely water yield (*WY*), actual evapotranspiration (ET_a), and groundwater recharge (*GR*), represent on average 35%, 49%, and 16% of the annual mean rainfall depth (*R*=1,229 mm). The annual rainfall depths for the other two scenarios (only two seasons without the transition season) shift down to 988 mm (dry scenario) and up to 1,393 mm (wet scenario), thus affecting

the water balance. When the dry season lasts eight months (dry scenario), water yield, actual evapotranspiration, and groundwater recharge decrease by 116 mm, 60 mm, and 66 mm, respectively, when compared to the reference scenario.

Please insert Table 4 here

In contrast, when the wet season lasts eight months (wet scenario), the water yield, actual evapotranspiration, and groundwater recharge increase by 93 mm, 21 mm, and 54 mm, respectively, when compared to the reference scenario. Water yield, actual evapotranspiration, and groundwater recharge represent on average 32%, 55%, and 13% of the annual rainfall depth in the extreme dry season (dry scenario), and 38%, 45%, and 18% of annual rainfall depth in the extreme wet season (wet scenario).

Decomposition of the annual results into the seasonal components highlights other interesting features that are shown in Fig. 10 (rainfall and potential evapotranspiration forcings) and in Fig. 11 (main water balance components). For the reference scenario the seasonal rainfall depth is 201 mm, 436 mm, and 593 mm for the dry, transition, and wet seasons, respectively, representing 16%, 35%, and 48% of the total annual rainfall (see Fig. 10a). Water yield depths span from 44 mm during the dry season to 251 mm during the rainy season (see Fig. 11a). Almost 60% of annual water yield occurs over the wet season, about 30% in the transition season, and about 10% in the dry season. In contrast, the actual evapotranspiration depths are higher than rainfall depths in the dry season (269 mm) and lower than rainfall depths during the transition (226 mm) and rainy (110 mm) seasons (see Fig. 11a).

Please insert Fig. 10 here

Please insert Fig. 11 here

Over the dry scenario (see Figs. 10b and 11b), the months belonging to the transition season become drier-than-normal. The total rainfall depths over the dry and wet seasons are 397 mm and 590 mm, respectively, whereas the extreme drought anomaly induces precipitation loss only in the dry season with a considerable decrease of 239 mm of rainfall

depth (Fig. 10b). The consequences of this situation on the average water balance components in the prolonged dry season lead to significant deficits (Fig. 11b). Water yield loss over the dry season is 93 mm, which represents 50% of water yield obtained for the dry and transition seasons in the reference scenario. The wet season (from November to February) provides about 590 mm of water yield per year. The water loss by actual evapotranspiration is limited and represents only 10% of ET_a obtained for the dry and transition seasons in the reference scenario (Fig. 11b).

In the wet scenario (see Fig. 10c and Fig. 11c), the months belonging to the transition season become wet (8 wet months and 4 dry months). Total rainfall depths in the dry and wet seasons are 200 mm and 1,193 mm (Fig. 10c). Rainfall depth increases by 164 mm in the wet season (+14% compared with that obtained in the wet and transition seasons in the reference scenario). Water yield gain in the wet season is 89 mm which represents 20% of water yield obtained in the wet and transition seasons in the reference scenario (Fig. 11c). The water lost by actual evapotranspiration is negligible.

5.4. Effects of seasonal rainfall anomalies on water balance when using the dynamic approach

The second approach to assessing the effect of rainfall seasonality extremes on water balance components is based on the stochastic generation of the wet season durations from their normal distribution (see Fig. 9b). This approach helps classify the results within a probabilistic framework according to the following rainy period duration classes: 3-4 months, 4-5 months, 5-6 months, 6-7 months, 7-8 months. Seasonal extremes (3-4 months and 7-8 months) have very low probabilities of occurrence (0.60% and 0.30%, respectively). Nonetheless, it is interesting to analyze the effect of rainfall variability on water yield (WY), actual evapotranspiration (ET_a) and groundwater recharge (GR). The most probable (62%) situation occurs when the rainy period lasts 5-6 months. Under these circumstances, the mean annual rainfall depth is 1,275 mm, whereas WY, ET_a, and GR represent 35%, 49%, and 16% of annual average rainfall depth, respectively. These percentages are very close to those observed in the reference scenario of the static approach. If the wet season shortens by one month (23% probability), the mean annual rainfall depth decreases by 62 mm, whereas water yield depth by 33 mm (−7%). In contrast, if the wet season is made up of 6-7 months (14% probability), the annual mean rainfall depth increases by 51 mm and water yield by 27 mm (+6%).

394   Extreme dry and extreme wet situations reflect similar results obtained from the dry and wet scenarios presented above.

395   A prolonged drought (i.e. rainy period only 3-4 months long) leads to an average rainfall loss of 130 mm per year

396   inducing an appreciable annual decrease in both water yield (−68 mm) and groundwater recharge (−30 mm). A

397   prolonged wet season (i.e. lasting 7-8 months), instead, causes average rainfall to gain approximately 108 mm per year,

398   yielding annual increases in both water yield (+59 mm) and groundwater recharge (+12 mm). It is worth noting that the

399   duration of the rainy period does not seem to exert a major control on the water balance. Pearson's linear correlation

400   coefficients between duration and average annual rainfall, water yield, and actual evapotranspiration are 0.22, 0.20, and

401   0.11, respectively.

402   *Please insert Table 5 here*

403   *Please insert Fig. 12 here*

404   Assuming that the long-term mean annual precipitation can be partitioned into the mean annual actual

405   evapotranspiration and mean annual water yield, according to the Budyko framework we assume that larger values of

406   the dryness index (drier climate conditions; $ET_p/R > 1$) induce a greater proportion of rainfall that is partitioned to ET_a.

407   In contrast, data on the left-hand side of the Budyko curve will be characterized by a greater proportion of rainfall that

408   is partitioned to water yield. Fig. 12 shows the Budyko plot of the dryness index (ET_p/R) versus the evaporative index

409   (ET_a/R) together with the Budyko curve (solid garnet line). In this plot we depict the data points (colored dots) for the

410   five different durations of the rainy period in UARC obtained by the dynamic approach. The first comment to be made

411   is that all of these data points gather within the energy-limited region of the Budyko plot, with the longest rainy period

412   (blue dot) favoring conditions of greater discharges (evaporative index $ET_a/R = 0.45$) and the shortest rainy period

413   (droughts indicated by the red dot) inducing higher evapotranspiration fluxes (evaporative index $ET_a/R = 0.54$). The

414   latter situation shows that on average the Upper Alento River catchment is characterized by relatively good storage of

415   soil-water made possible by the hydraulic properties of the soils and the large portion of shrub spots and forest areas

416   (mostly deciduous chestnut forests and olive orchards), together with a good amount of annual precipitation in a hilly

417   and mountainous zone in southern Italy. However, it may also be noted that all of these data points cluster below the

418   Budyko curve (Williams et al., 2012). The observed departure below the Budyko curve may be due to several reasons.

419   Allowing for the Budyko assumptions for water balance, the present study refers to a long time scale (90 years), but a

420   relatively small spatial scale since UARC has a drainage area of 102 km^2. In fact, rainfall seasonality (i.e. intra-annual

421   variability) may be just one of the major factors that could have led to a departure from the Budyko curve. The typical

422   Mediterranean climate, which is characterized by precipitation being out-of-phase with potential evapotranspiration, is

423   also singled out as a cause of the deviations we observed in our case study from the Budyko curve (Milly, 1994).

424   Normal situations, characterized by a wet season lasting 5-6 months (green dot), lead to rainfall being partitioned into

425   49% ET_a, as indicated by the evaporative index value of 0.49. We hereby recall that this study is based on the

426   assumption that the catchment response is not affected by human interferences and their feedbacks (land-use change,

427   change in soil hydraulic properties, enhanced evapotranspiration induced by global warming, etc.), but only by changes

428   in rainfall seasonality which, of course, can undermine Budyko's implicit assumption of temporal steady-state (Feng et

429   al., 2012; Troch et al., 2013).

430   *Please insert Fig. 13 here*

431   *Please insert Table 6 here*

432   The relationships between the seasonal dryness index and water yield to rainfall ratio (*WY/R*) are affected by the

433   duration of the wet season and are depicted in Fig. 13. The coefficients of the exponential regression models with their

434   corresponding R^2 values pertaining to the wet or dry season are reported for each duration class of the rainy period in

435   Table 6. The exponential curves in the wet season (see plot 13a) are virtually parallel, yielding, for a fixed ET_p/R, more

436   *WY/R* as the duration of the rainy period increases from 3-4 months to 7-8 months. In contrast, the exponential

437   regression curves belonging to the dry season (see plot 13b) explain only a small amount of the variations of *WY/R* in

438   response to the dryness index and all seem quite insensitive to rainfall seasonality. Only the exponential model

439 pertaining to the dry season and for the smaller duration of the rainy period (3-4 months) explains slightly less than 50%

440 of the variability of ET_p/R for the study catchment.

441

442 **6. Conclusions**

443 Capturing the relationship between precipitation and catchment-scale water balance components in a Mediterranean

444 context is a scientific challenge in view of expected increasing frequencies in extremes such as droughts and floods

445 induced by climate warming. On the one hand, intense and prolonged droughts induce a steep decline in water

446 availability for irrigation (with a subsequent decrease in crop productivity), domestic use (especially for the tourist

447 sector), clean power generation, to mention just a few. On the other hand, projected increments in runoff and flooding

448 induce higher-than-normal risk of landslides and soil erosion, compromising the local economy and leading to

449 unprecedented hazards for a vulnerable population. Therefore, countries across the Mediterranean region are being

450 forced to pursue drastic adaptive options which in turn depend on modeling scenarios which can be performed by using

451 hydrological models. Indeed, scenarios need to rely on adequate rainfall modeling within the hydrological year by

452 generating multiple data sets of reliable daily rainfall time series drawn from statistical distributions derived from long-

453 term observations. Nonetheless, a key is first to define rainfall seasons, and then optimize parameters featuring in the

454 best statistical distribution describing rainfall data distribution in each season. If this exercise is well posed, one can

455 capture realistic rainfall dynamics occurring in the water balance simulated by a numerical model. Within this

456 framework, the aim of this study is to contribute in understanding the impact of rainfall seasonality and its anomalies on

457 the water balance components by providing reliable and robust scenario-based projections, based on the use of well-

458 posed hydrological models.

459 This study presented a pilot area (UARC in southern Italy) in the Mediterranean region. We applied the SWAT model

460 that was calibrated and validated in a previous paper using a large amount of environmental data and maps (Nasta et al,

461 2017). Moreover, the availability of a long-term time series of daily rainfall data (almost one century) allowed us to

detect rainfall seasonality by using a static and a dynamic approach. In both approaches we apply the SWAT model to evaluate the sensitivity of hydrological water balance components to rainfall seasonality, using as input synthetic rainfall time series generated by a Poisson process with two parameters that characterize daily rainfall occurrences and daily rainfall depth in each season. In the static approach, dry or wet anomalies are considered when the transition seasons turn into dry or wet seasons. The advantage of this approach lies in its simplicity and easy reproducibility in other sites. However, it can be considered only an artifact based on criteria to group monthly rainfall amounts that might be subjective. In the dynamic approach, the seasonal anomalies occur on the tails of the normal distribution of the wet season duration. Although this approach seems statistically sound, the main disadvantage is the fact that it requires long-term historical rainfall time-series of daily rainfall data that are unlikely to be available in most weather stations across the Mediterranean region. In this study, both approaches concurred on understanding the impact of seasonal rainfall anomalies on catchment-scale water balance components.

Our results show a drought anomaly (i.e. a prolonged duration of the dry season) in just one single year potentially leads to a decrease of even about a fifth of the annual average rainfall and induces a drastic decline in average annual amounts of water yield, actual evapotranspiration, and groundwater recharge. Conversely, an exceptional prolonged wet season is likely to cause a considerable increase in annual average rainfall, hence about a one-third rise in annual average water yield as well as enhanced groundwater recharge. In the dynamic approach, we demonstrated that the implicit assumption of a temporal steady-state in the Budyko relation approach is sensitive to rainfall seasonality. The Budyko evaporative index spans from 0.45 to 0.54 when the wet season lasts from 7-8 months up to 3-4 months. Moreover, it is possible to identify distinct season-dependent regression equations linking seasonal water yield to the dryness index over the wet season.

In conclusion this paper provides a framework to analyze the effects of rainfall seasonality changes on the hydrological water budget and partition, while providing some preliminary results that can be representative for Mediterranean catchments. Finer analyses can be performed by considering consecutive years of prolonged drought episodes and/or by

485   adding the effects of temperature trends, which obviously affect potential evapotranspiration forcing and in principle

486   can produce a further feedback on precipitation cycles. These still unexplored issues will form the subject of future

487   research investigation and forthcoming communications.

488   **7. Appendix**

489   We set k and m as counters for the hydrological year and the 12 months in each year, respectively. The annual rainfall,

490   R_k, and associated monthly probability distribution, $p_{k,m}$, are defined as:

491     $R_k = \sum_{m=1}^{12} r_{k,m}$ (A1)

492     $p_{k,m} = \dfrac{r_{k,m}}{R_k}$ (A2)

493   where $r_{k,m}$ represents the rainfall depth recorded in the m-th month in the k-th year.

494   The relative entropy, D_k, is calculated in each hydrological year, k, as:

495     $D_k = \sum_{m=1}^{12} p_{k,m} \, log_2 \left(\dfrac{p_{k,m}}{q_m} \right)$ (A3)

496   where q_m is equal to 1/12 (uniform distribution). This statistical index quantifies the distribution of monthly rainfall

497   within each hydrological year. Finally, the dimensionless seasonality index (DSI_k) in each hydrological year, k, is given

498   by:

499     $DSI_k = D_k \dfrac{R_k}{\bar{R}_{max}}$ (A4)

500   where $\bar{R}_{max}$ is maximum $\bar{R}$. This way DSI_k is zero when rainfall is uniformly distributed throughout the year and

501   reaches its maximum value $log_2 12$ when rainfall is concentrated in a single month.

502   According to Feng et al. (2013), the magnitude (R_k) represents annual rainfall whereas the centroid (C_k) and the spread

503   (Z_k) indicate timing and duration of the wet season, respectively, and are calculated in each hydrological year k as:

504 $\quad C_k = \frac{1}{R_k} \sum_{m=1}^{12} m r_{k,m}$ $\hspace{6cm}$ (A5)

505 $\quad Z_k = \sqrt{\frac{1}{R_k} \sum_{m=1}^{12} |m - C_k|^2 r_{k,m}}$ $\hspace{5cm}$ (A6)

506

507 **Acknowledgments**

508 The study reported in this paper was partially supported by the MiUR-PRIN Project "Innovative methods for water

509 resources management under hydro-climatic uncertainty scenarios" (grant 2010JHF437). The Director of the Consorzio

510 di Bonifica Velia, Marcello Nicodemo, is also acknowledged for his support in providing the datasets recorded at the

511 Piano della Rocca earth dam. Roberto Deidda acknowledges the financial support received from the Sardinia Regional

512 Authority under grant L.R. 7/2007, funding call 2017, CUP: F76C18000920002.

513

514 **References**

515 Abbott, B.W., Bishop, K.H., Zarnetske, J.P., Minaudo, C., Chapin, F.S., Krause S., Hannah, D.M., Conner, L., Ellison,

516 $\quad$ D., Godsey, S.E., et al.: Human domination of the global water cycle absent from depictions and perceptions, Nat.

517 $\quad$ Geosci., doi: 10.1038/s41561-019-0374-y, 2019.

518 Adla, S., Tripathi, S., and Disse, M.: Can we calibrate a daily time-step hydrological model using monthly time-step

519 $\quad$ discharge data?, Water, 11, 1750, doi:10.3390/w11091750, 2019.

520 Allen, R.G., Pereira, L.S., Raes, D., and Smith, M.: Crop Evapotranspiration: Guidelines for Computing Crop Water

521 $\quad$ Requirements., Food and Agriculture Organization of the United Nations, 1998.

522 Ayoade, J.O.: The seasonal incidence of rainfall, Weather 25, 414-418, https://doi.org/10.1002/j.1477-

523 $\quad$ 8696.1970.tb04132, 1970.

524 Apurv, T., Sivapalan, M., and Cai, X.: Understanding the role of climate characteristics in drought propagation, Water

525 $\quad$ Resourc. Res., 53, 9304–9329. https://doi.org/10. 1002/2017WR021445, 2017.

526 Arnold, J.G., Srinivasan, R., Muttiah, R.S., and Williams, J.R.: Large area hydrologic modeling and assessment part I:

527 $\quad$ model development, J. Am. Soc. Water Resour. Assoc., 34 (1), 73–89, 1998.

528 Bari, S.H., Hussain, M.M., and Husna, N.E.A.: Rainfall variability and seasonality in northern Bangladesh, Theor.

529 $\quad$ Appl. Climatol., https://doi.org/10.1007/s00704-016-1823-9, 2016.

530   Budyko, M.I.: Climate and Life., Academic Press, New York, 1974.

531   Caracciolo D., Deidda R., and Viola F.: Analytical estimation of annual runoff distribution in ungauged seasonally dry
532   basins based on a first order Taylor expansion of the Fu's equation, Adv. Water Resourc., 109, 320-332,
533   https://doi.org/10.1016/j.advwatres.2017.09.019, 2017.

534   Corona, R., Montaldo, N., and Albertson, J.D.: On the Role of NAO-Driven Interannual Variability in Rainfall
535   Seasonality on Water Resources and Hydrologic Design in a Typical Mediterranean Basin, J. Hydrometeorol., 19,
536   485-498, doi: 10.1175/jhm-d-17-0078.1, 2018.

537   de Lavenne, A., and Andréassian, V.: Impact of climate seasonality on catchment yield: A parameterization for
538   commonly-used water balance formulas, J. Hydrol., 558, 266-274, 2018.

539   Deidda, R.: An efficient rounding-off rule estimator: Application to daily rainfall time series, Water Resour. Res., 43,
540   W12405, doi:10.1029/2006WR005409, 2007.

541   Deidda, R.: A multiple threshold method for fitting the generalized Pareto distribution to rainfall time series, Hydrol.
542   Earth Syst. Sci., 14, 2559–2575, 2010.

543   Domínguez-Castro, F., Vicente-Serrano, S.M., Tomás-Burguera, M., Peña-Gallardo, M., Beguería, S., El Kenawy, A.,
544   Luna, Y., and Morata, A.: High-spatial-resolution probability maps of drought duration and magnitude across Spain,
545   Nat. Hazards Earth Syst. Sci., 19, 611–628, 2019.

546   Eagleson, P. S.: Dynamics of flood frequency, Water Resour. Res., 8, 878–898, 1972.

547   Feng, X., Porporato, A., and Rodriguz-Iturbe, I.: Changes in rainfall seasonality in the tropics, Nat. Clim. Change,
548   https://doi.org/10.1038/nclimate1907, 2013.

549   Feng, X., Vico, G., and Porporato, A.: On the effects of seasonality on soil water balance and plant growth, Water
550   Resour. Res., 48, W05543, doi:10.1029/2011WR011263, 2012.

551   Hargreaves, G.L., Hargreaves, G.H., and Riley, J.P.: Irrigation water requirements for Senegal river basin, J. Irrig.
552   Drain. Eng., 111, 265–275, 1985.

553   Hanel, M., Rakovec, O., Markonis, Y., Máca, P., Samaniego, L., Kyselý, J., and Kumar, R.: Revisiting the recent
554   European droughts from a long-term perspective, Scientific Reports, 8:9499, doi:10.1038/s41598-018-27464-4,
555   2018.

556   Hayes, M., Wilhite, D.A., Svoboda, M., and Vanyarkho, O.: Monitoring the 1996 drought using the Standardized
557   Precipitation Index, Bull. Am. Meteorol. Soc., 80, 429-438, 1999.

558   Kendall, M.G.: Rank Correlation Measures, Charles Griffin: London, 1975.

559   Kutiel, H., and Trigo, R.M.: The rainfall regime in Lisbon in the last 150 years, Theor. Appl. Climatol., doi
560   10.1007/s00704-013-1066-y, 2013.

561 IPCC, Climate change, 2013: the physical science basis. Contribution of working group I to the fifth assessment report
562   of the intergovernmental panel on climate change. Cambridge, United Kingdom and New York, USA: Cambridge
563   University Press.

564 Laaha, G., Gauster, T., Tallaksen, L. M., Vidal, J.-P., Stahl, K., Prudhomme, C., Heudorfer, B., Vlnas, R., Ionita, M.,
565   Van Lanen, H. A. J., Adler, M.-J., Caillouet, L., Delus, C., Fendekova, M., Gailliez, S., Hannaford, J., Kingston, D.,
566   Van Loon, A. F., Mediero, L., Osuch, M., Romanowicz, R., Sauquet, E., Stagge, J. H., and Wong, W. K.: The
567   European 2015 drought from a hydrological perspective, Hydrol. Earth Syst. Sci., 21, 3001–
568   3024,https://doi.org/10.5194/hess-21-3001-2017, 2017.

569 Lilliefors, H.W.: On the Kolmogorov-Smirnov test for normality with mean and variance unknown, J. Am. Stat. Assoc.,
570   62, 399–402, 1967.

571 Livada, I., and Asimakopoulos, D.N.: Individual seasonality index of rainfall regimes in Greece, Clim. Res., 28, 155–
572   161, 2005.

573 Mann, H.B.: Non-parametric tests against trend, Econometrica, 13, 245-259, 1945.

574 Markham, C.G.: Seasonality of precipitation in the United States, Ann. Am. Assoc. Geogr., 60, 593–597,
575   https://doi.org/10.1111/j.1467-8306.1970.tb00743.x, 1970.

576 Mariotti, A., Zeng, N., Yoon, J.-H., Artale, V., Navarra, A., Alpert, P., and Li, L.: Mediterranean water cycle changes:
577   transition to drier 21st century conditions in observations and CMIP3 simulations, Environ. Res. Lett., 3,
578   doi:10.1088/1748-9326/3/4/044001, 2008.

579 Martin-Vide, J.: Spatial distribution of a daily precipitation concentration index in Peninsular Spain, Int. J. Climatol.,
580   24, 959-971, 2004.

581 McKee, T.B., Doesken, N.J., and Kleist, J.: The relationship of drought frequency and duration to time scales. In
582   "Eighth conference on applied climatology", pp. 17–22, Anaheim, California: American Meteorological Society,
583   1993.

584 Miller, S.N., Kepner, W.G., Mehaffey, M.H., Hernandez, M., Miller, R.C., Goodrich, D.C., Devonald, K.K., Heggem,
585   D.T., and Miller, W.P.: Integrating landscape assessment and hydrologic modeling for land cover change analysis, J.
586   Am. Water Resourc. Assoc., 38, 915-929, 2002.

587 Milly, P.C.D.: Climate, soil water storage, and the average annual water balance, Water Resour. Res., 30, 2143-2156,
588   1994.

589 Nasta, P., Romano, N., and Chirico, G.B.: Functional evaluation of a simplified scaling method for assessing the spatial
590   variability of the soil hydraulic properties at hillslope scale, Hydrol. Sci. J., 58, 1-13, 2013.

Nasta, P., Palladino, M., Ursino, N., Saracino, A., Sommella, A., and Romano, N.: Assessing long-term impact of land use change on hydrologic ecosystem functions in a Mediterranean upland agro-forestry catchment, Sci. Total Environm., 605-606, 1070-1082, 2017.

Nasta, P., Sica, B., Mazzitelli, C., Di Fiore, P., Lazzaro, U., Palladino, M., and Romano, N.: How effective is information on soil-landscape units for determining spatio-temporal variability of near-surface soil moisture?, J. Agric. Eng., 49(3), 174-182, doi:10.4081/jae.2018.822, 2018.

Nasta, P., Boaga, J., Deiana, R., Cassiani, G., and Romano, N.: Comparing ERT- and scaling-based approaches to parameterize soil hydraulic properties for spatially distributed model applications, Adv. Water Resourc., 126, 155-167, 2019.

Nieuwolt, S.: Seasonal rainfall distribution in Tanzania and its cartographic representation, Erdkunde, 28, 186–194, 1974.

Oliver, J.E.: Monthly precipitation distribution: A comparative index, Prof. Geogr., 32, 300–309, 1980.

Hosking, J.R.M.: L-moments: Analysis and estimation of distributions using linear combinations of order statistics, J. Royal Stat. Soc., Series B (Methodological), 52, 105-124, 1990.

Pascale, S., Lucarini, V., Feng, X., Porporato, A., and Hasson, S.: Analysis of rainfall seasonality from observations and climate models, Clim. Dyn., 44, 3281–3301, 2015.

Pascale, S., Lucarini, V., Feng, X., Porporato, A., and Hasson, S.: Projected changes of rainfall seasonality and dry spells in a high greenhouse gas emissions scenario, Clim. Dyn., 46, 1331-1350, 2016.

Paz, S., and Kutiel, H.: Rainfall regime uncertainty (RRU) in an eastern Mediterranean region — a methodological approach, Isr. J. Earth Sci., 52: 47–63, 2003.

Piccarreta, M., Pasini, A., Capolongo, D., and Lazzari, M.: Changes in daily precipitation extremes in the Mediterranean from 1951 to 2010: the Basilicata region, southern Italy, Int. J. Climatol., 33, 3229–3248, 2013.

Potter, N.J., Zhang, L., Milly, P.C.D., McMahon, T.A., and Jakeman, A.J.: Effects of rainfall seasonality and soil moisture capacity on mean annual water balance for Australian catchments, Water Resour. Res., 41, W06007, doi:10.1029/2004WR003697, 2005.

Pryor, S.C., and Schoof, J.T.: Changes in the seasonality of precipitation over the contiguous USA, J. Geophys. Res., 113, D21108. https://doi.org/10.1029/2008JD010251, 2008.

Raziei, T.: An analysis of daily and monthly precipitation seasonality and regimes in Iran and the associated changes in 1951–2014, Theor. Appl. Climatol., pp.134:913–934 https://doi.org/10.1007/s00704-017-2317-0, 2018.

Rivoire, P., Tramblay, Y., Neppel, L., Hertig, E., and Vicente-Serrano, S.M.: Impact of the dry-day definition on Mediterranean extreme dry-spell analysis, Nat. Hazards Earth Syst. Sci., 19, 1629–1638, 2019.

622 Rodríguez-Iturbe, I., Febres de Power, B., and Valdés, J.B.: Rectangular pulses point process models for rainfall: Analysis of empirical data, J. Geophys. Res., https://doi.org/10.1029/JD092iD08p09645, 1987.

624 Romano N., Nasta, P., Bogena, H.R., De Vita, P., Stellato, L., and Vereecken, H.: Monitoring hydrological processes for land and water resources management in a Mediterranean ecosystem: the Alento River catchment observatory, Vadose Zone J., 17, 180042. doi:10.2136/vzj2018.03.0042, 2018.

627 Sahany, S., Mishra, S. K., Pathak, R., and Rajagopalan, B.: Spatiotemporal variability of seasonality of rainfall over India, Geophys. Res. Lett., 45, 7140-7147, 2018.

629 SCS, 1972. Hydrology. Section 4 in National Engineering Handbook. Washington, D.C.: USDA Soil Conservation Service.

631 Sumner, G., Homar, V., and Ramis, C.: Precipitation seasonality in eastern and southern coastal Spain, Int. J. Climatol., 21, 219–247, https://doi.org/10.1002/joc.600, 2001.

633 Troch, P.A, Carrillo, G., Sivapalan, M., Wagener, T., and Sawicz, K.: Climate-vegetation-soil interactions and long-term hydrologic partitioning: signatures of catchment co-evolution, Hydrol. Earth Syst. Sci., 17, 2209–2217, 2013.

635 Van Loon, A.F., Tijdeman, E., Wanders, N., Van Lanen, H.A.J., Teuling, A.J., and Uijlenhoet, R.: How climate seasonality modifies drought duration and deficit, J. Geophys. Res. Atmos., 119, 4640–4656, doi:10.1002/2013JD020383, 2014.

638 Veneziano, D., and Iacobellis, V.: Multiscaling pulse representation of temporal rainfall, Water Resour. Res., 38, 1138, 10.1029/2001WR000522, 2002.

640 Viola, F., Caracciolo, D., Forestieri, A., Pumo, D., and Noto, L.: Annual runoff assess- ment in arid and semi-arid Mediterranean watersheds under the Budyko's framework, Hydrol. Process., 31 (10), 1876–1888, http://dx.doi.org/10.1002/hyp.11145, 2017.

643 Vogel, R.M., and Fennessey, N.M.: L moment diagrams should replace product moment diagrams, Water Resourc. Res., 29, 1745-1752, 1993.

645 Walsh, R.P.D., and Lawler, D.M.: Rainfall seasonality: description, spatial patterns and change through time, Weather 36, 201–208, https://doi.org/10.1002/j.1477-8696.1981.tb05400.x, 1981.

647 Williams, C. A., Reichstein, M., Buchmann, N., Baldocchi, D., Beer, C., Schwalm, C., Wohlfahrt, G., Hasler, N., Bernhofer, C., Foken, T., Papale, D., Schymansky, S., and Schaefer, K.: Climate and vegetation controls on the surface water balance: Synthesis of evapotranspiration measured across a global network of flux towers, Water Resour. Res., 48, W06523, doi:10.1029/2011WR011586, 2012.

651 Zhang, L.J., and Qian, Y.F.: Annual distribution features of precipitation in China and their interannual variations, Acta Meteorol. Sin., 17, 146–163, 2003.

653

Figures
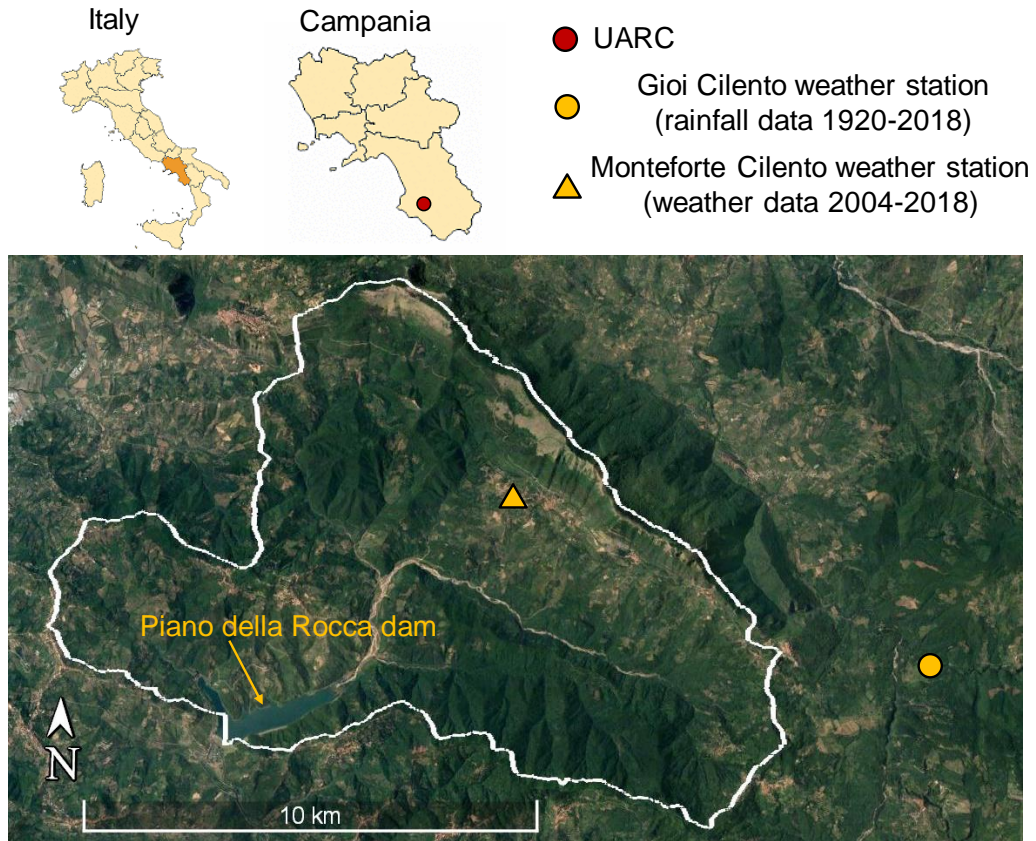
Figure 1:Geographical position of the Upper Alento River Catchment (UARC) in Campania (southern Italy) with the locations of the weather stations of Gioi Cilento and Monteforte Cilento. This figure was adapted from © Google Maps
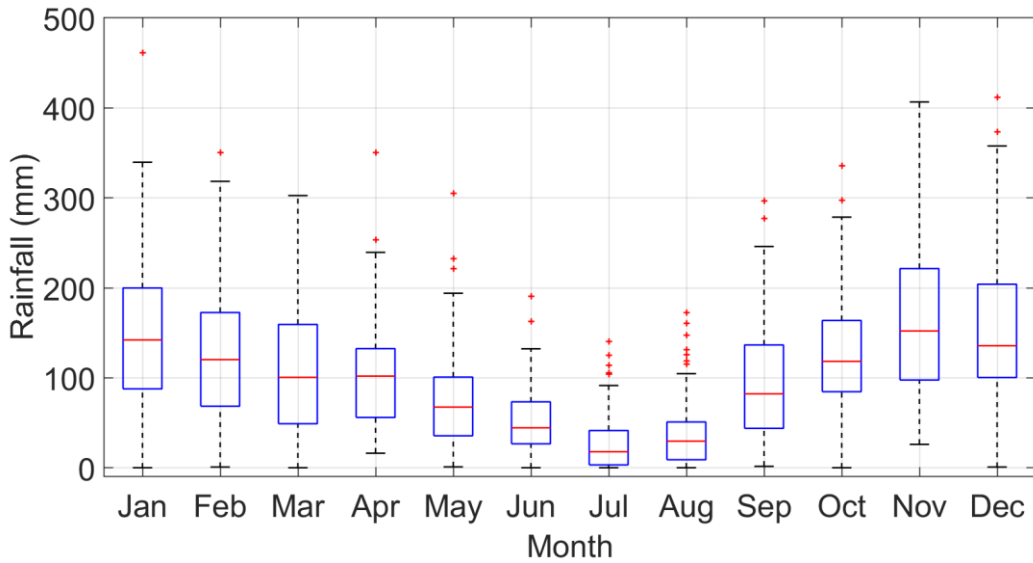
Figure 2: Box plots of monthly rainfall depths recorded at the Gioi Cilento weather station (1920-2018).
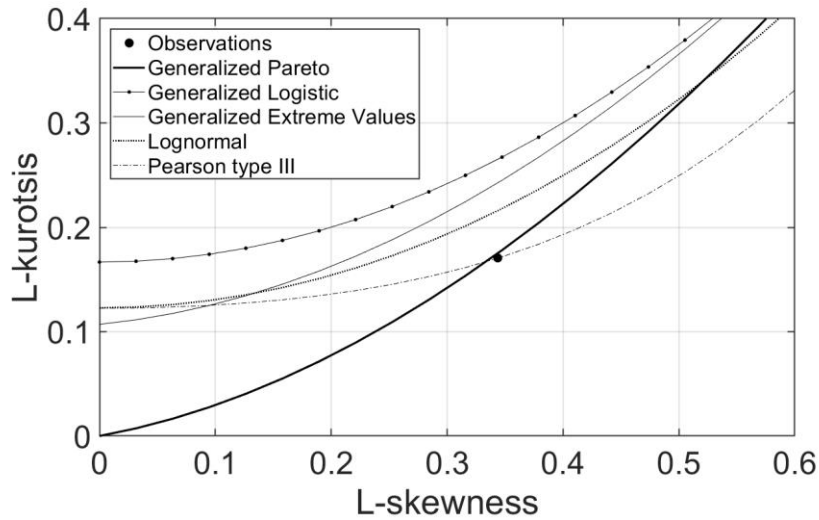
Figure 3: Theoretical L-moment ratio of common distribution models, as compared to the sample L-moment ratios of daily rainfall time series at the Gioi Cilento weather station (large filled circle).
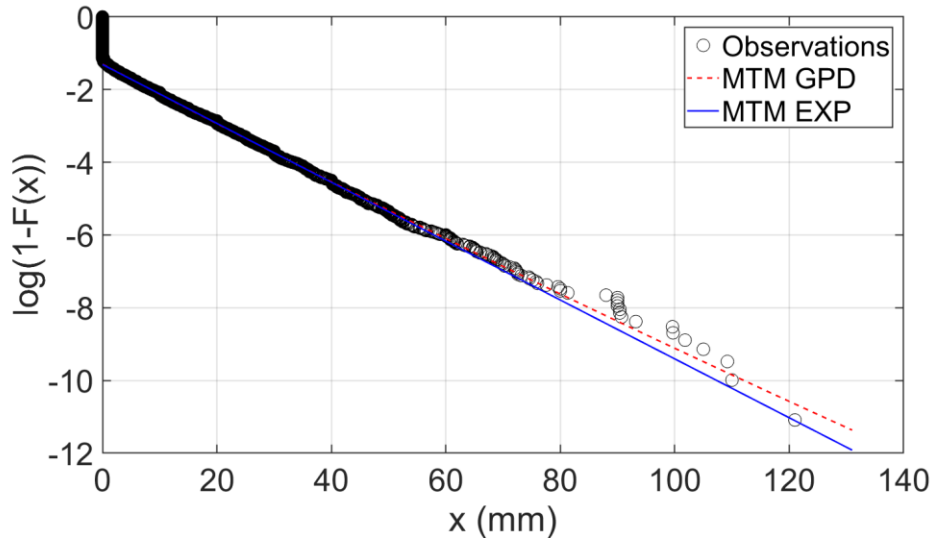
Figure 4: Exponential probability plot of empirical and fitted cumulative distribution functions of daily rainfall depths collected at the Gioi Cilento weather station.
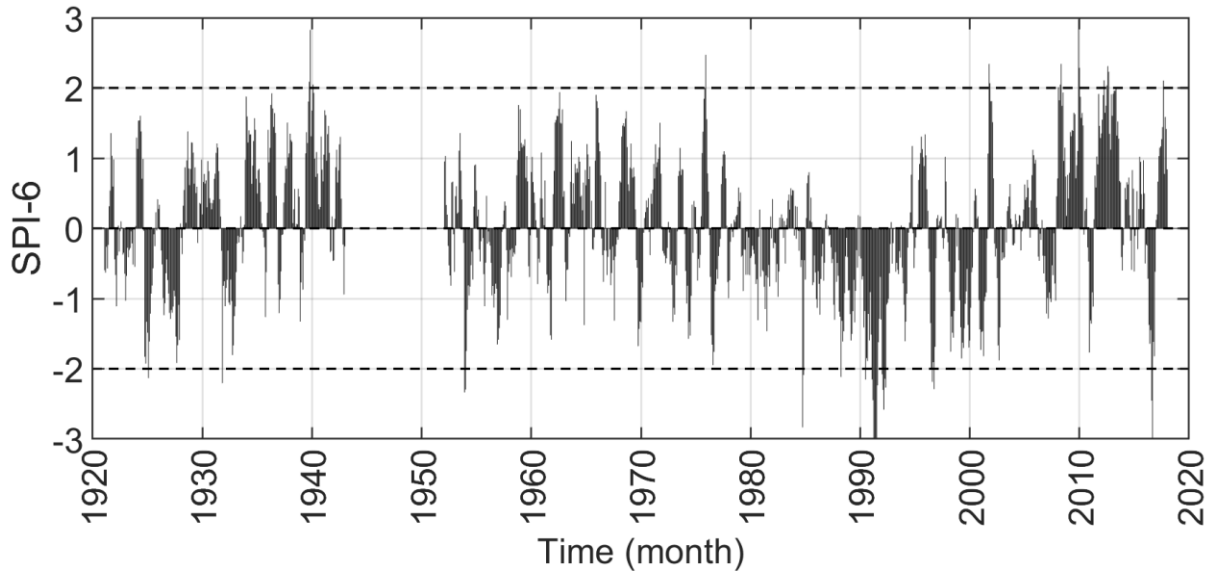
Figure 5: Temporal evolution of SPI-6 spanning from 1920 to 2018 (rainfall data were recorded at the Gioi Cilento weather station).
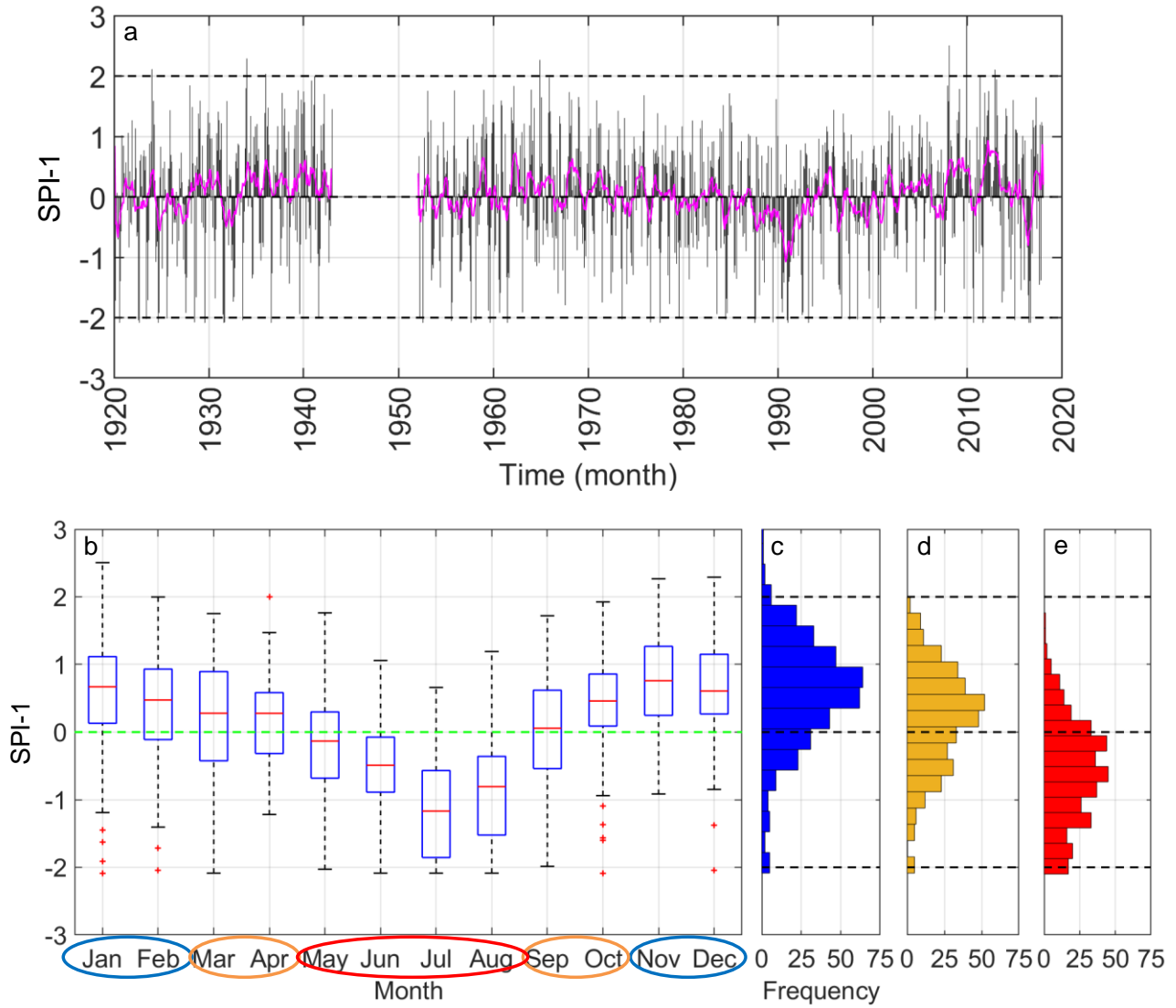
Figure 6: a) Temporal evolution of SPI-1 values (gray bars) and their 12-month moving average (magenta line) spanning from 1920 to 2018 in the static approach; b) Box plots of SPI-1 values and frequency distribution in the c) rainy period (blue histograms corresponding to Nov-Dec-Jan-Feb), d) transition period (yellow histograms corresponding to Mar-Apr-Sep-Oct), e) dry period (red histograms corresponding to May-Jun-Jul-Aug).
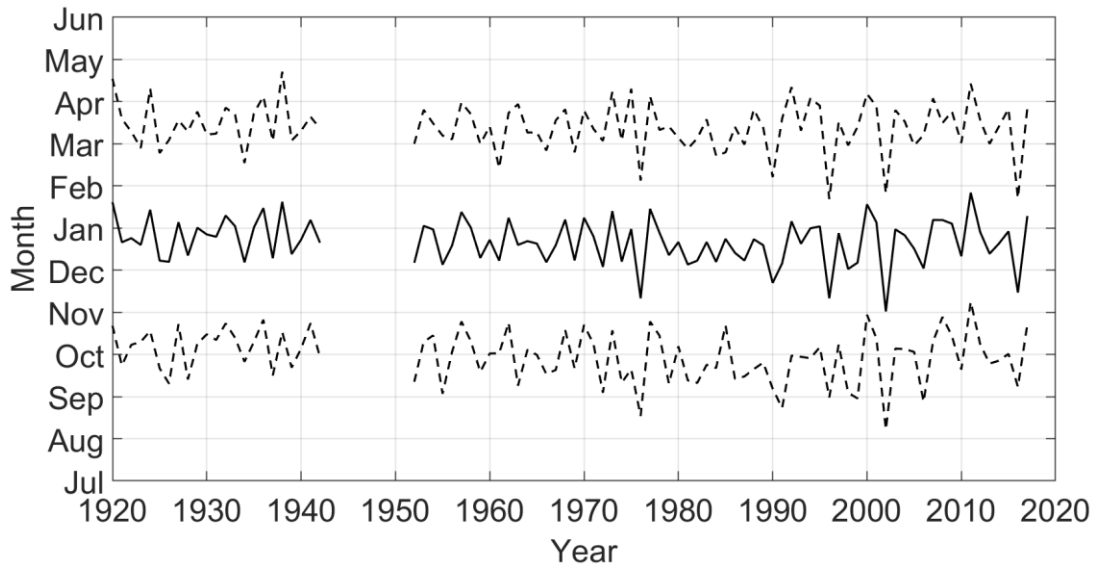
Figure 7: Temporal evolution of the centroid (or timing; solid line) and spread (or duration; dashed lines) of the wet seasons estimated as proposed by Feng et al. (2013) within the framework of the dynamic approach (rainfall data were recorded at the Gioi Cilento weather station).

.
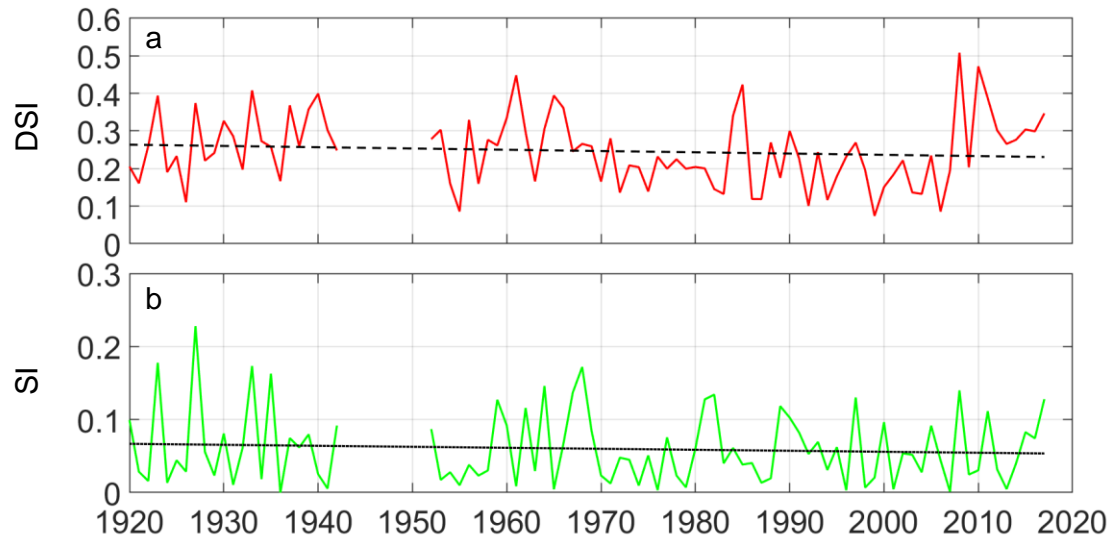
Figure 8: Temporal evolution of a) dimensionless seasonal index, DSI (Feng et al., 2013) represented by a red line with corresponding linear regression (dashed line); b) seasonality index, SI (Walsh and Lawler, 1981) represented by a green line with corresponding linear regression (dotted line).
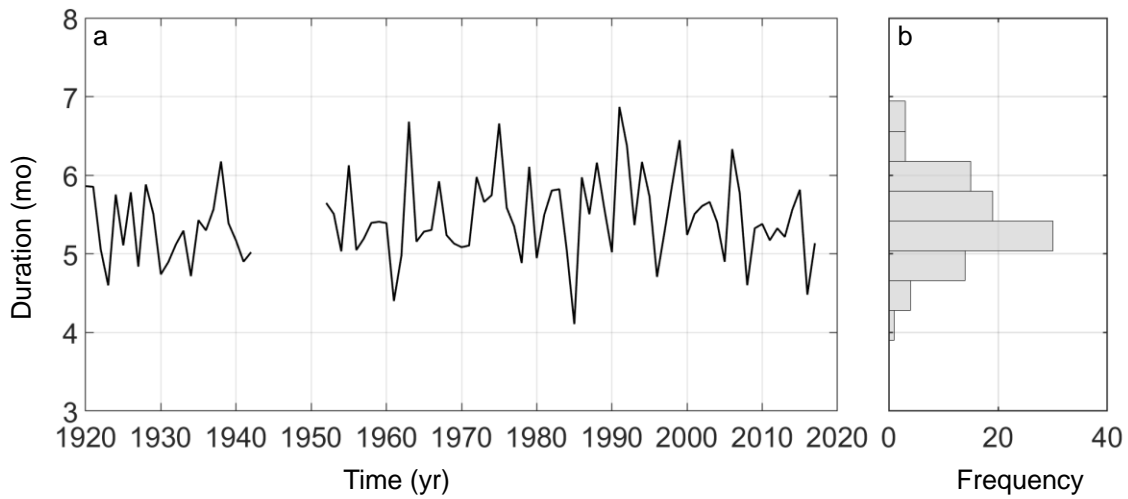
Figure 9: Time series (a) and frequency distribution (b) of durations of the rainy periods at the Gioi Cilento weather station in the dynamic approach.
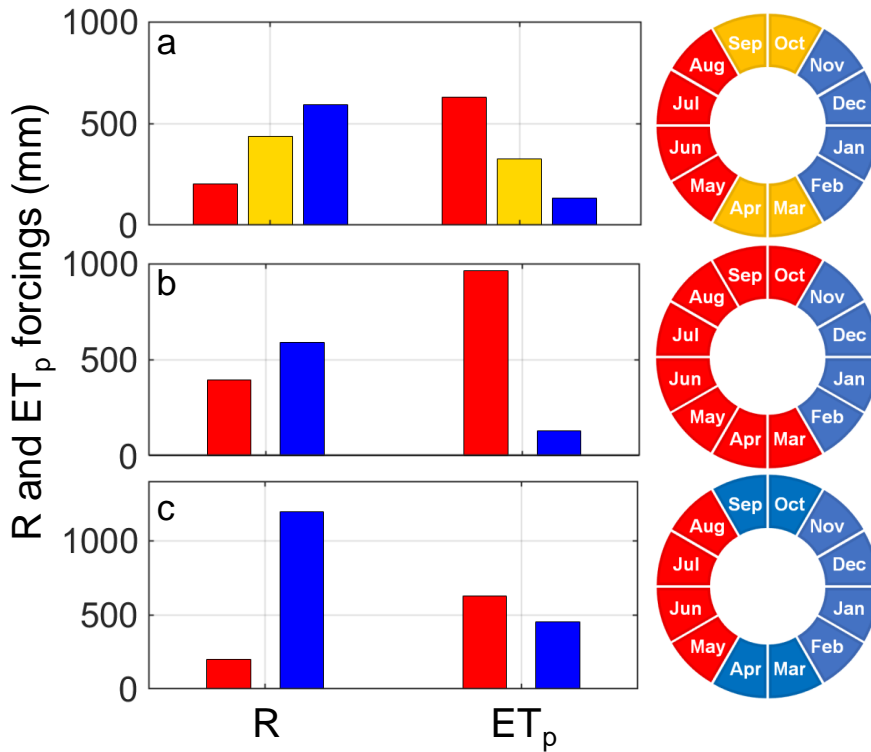
Figure 10: Rainfall and potential evapotranspiration forcings in the static approach, namely seasonal rainfall (R) and potential evapotranspiration (ET_p) in the dry (red bars), transition (orange bars), and wet season (blue bars). Three scenarios are presented: a) "reference scenario" with the dry, transition, and wet seasons all lasting 4 months; b)"dry scenario" with the dry and wet seasons lasting 8 and 4 months, respectively; c) "wet scenario" with the dry and wet seasons lasting 4 and 8 months, respectively.
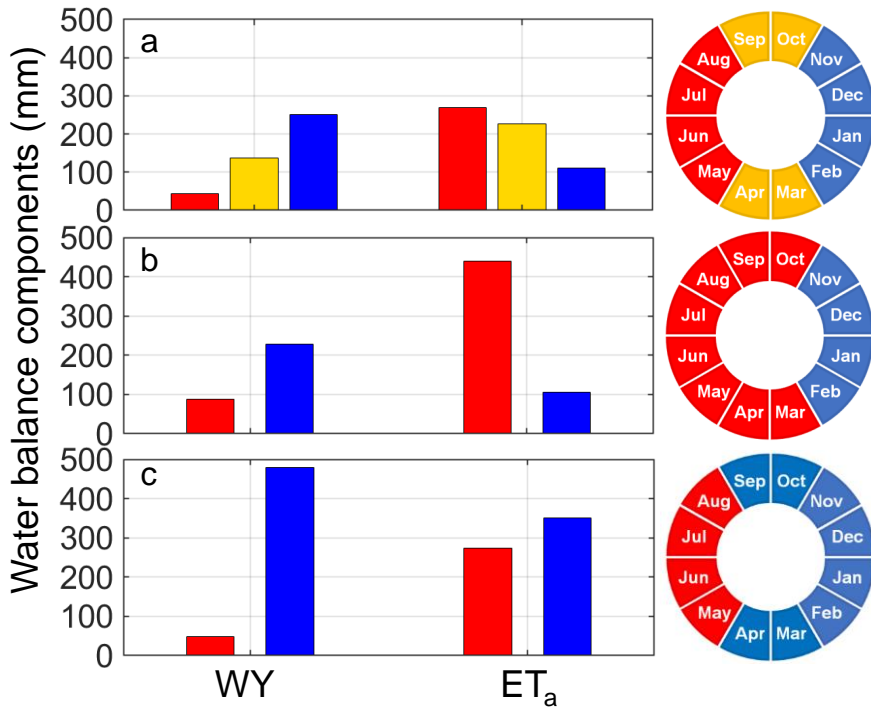
Figure 11: Main water balance components in the static approach, namely seasonal water yield (WY) and actual evapotranspiration (ET_a) in the dry (red bars), transition (orange bars), and wet season (blue bars). Three scenarios are presented: a) "reference scenario" with the dry, transition, and wet seasons all lasting 4 months; b) "dry scenario" with the dry and wet seasons lasting 8 and 4 months, respectively; c) "wet scenario" with the dry and wet seasons lasting 4 and 8 months, respectively.
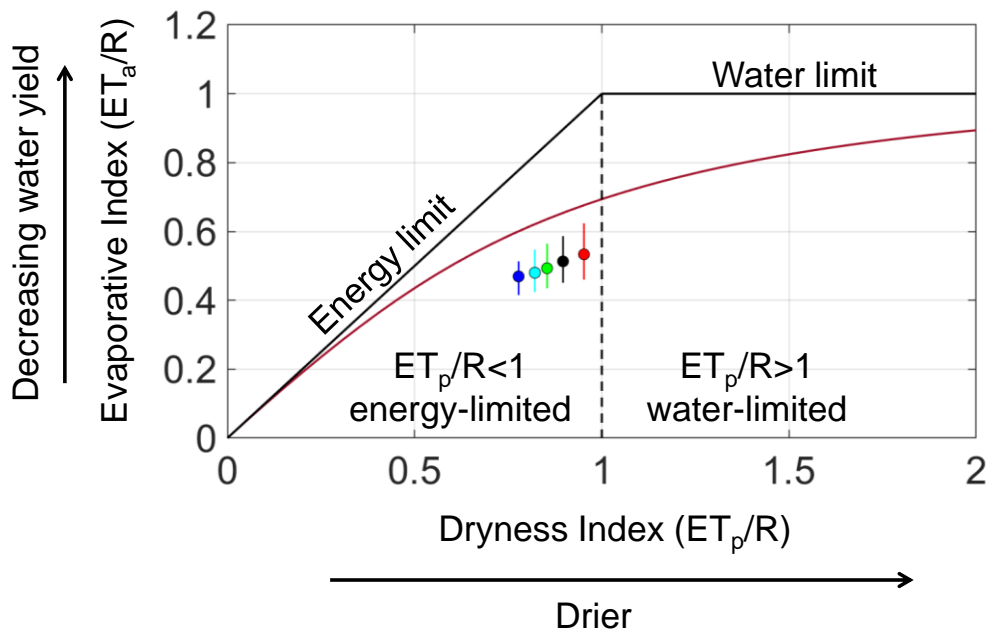
Figure 12: Budyko diagram relating the dryness index (ET_p/R) with the evaporative (ET_a/R) index classified according to the duration of the rainy period pertaining to the dynamic approach. Circles denote median and vertical colored lines represent the range between 5th and 95th percentiles of evaporative index (red, black, green, cyan and blue colors correspond to duration of the rainy period of 3-4, 4-5, 5-6, 6-7 and 7-8 months, respectively). Solid lines denote energy and water limits, the solid garnet line represents the Budyko curve (Budyko, 1974). The vertical dashed line separates left-hand side from right-hand side of the Budyko curve.
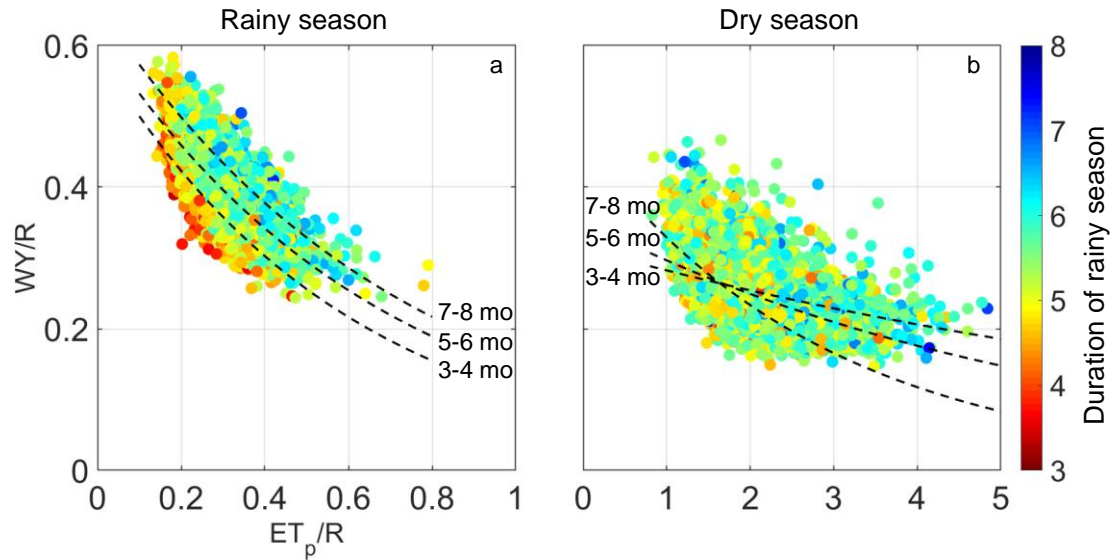
Figure 13: Relationship between dryness index and water yield to rainfall ratio (*WY/R*) on a seasonal basis and classified according to the duration of the wet season (from shortest to longest denoted by reddish and bluish colors in the color bar) pertaining to the dynamic approach for the wet season (plot 12a) and the dry season (plot 12b). The exponential regression equations are represented in both plots by the dashed black lines according to the duration of the rainy period.

Tables

Table 1: Descriptive statistics of the monthly and annual rainfall distributions recorded at the Gioi Cilento weather station during the period 1920-2018.

	mean	*median*	*min*	*max*	*Std. Dev.*	*CV*
	mm	mm	mm	mm	mm	%
Jan	145.6	141.65	0.0	461.2	81.6	56.0
Feb	128.1	120.25	0.8	350.1	76.3	59.6
Mar	112.9	101.1	0.0	302.6	73.4	65.0
Apr	102.5	101	16.2	350.6	59.5	58.0
May	75.2	67.6	1.1	304.8	56.6	75.2
Jun	52.8	45.3	0.0	190.9	38.2	72.3
Jul	29.8	17.6	0.0	140.4	32.8	110.0
Aug	39.7	30.3	0.0	210	42.8	107.7
Sep	94.4	81.9	1.6	296.8	63.0	66.7
Oct	126.8	118.8	0.0	335.5	70.3	55.4
Nov	166.9	152.2	26.0	613.2	94.9	56.9
Dec	154.6	134.55	0.8	411.8	85.1	55.1
Annual	1229.3	1198.3	478.6	2069.6	295.9	24.1

Table 2: Scenario set-up in the "*static*" approach. Duration and Poisson distribution parameters (η and λ) are reported for each of the considered scenarios.

	Dry season			Transition season			Wet season		
	months	η	λ	months	η	λ	months	η	λ
	-	mm	d^{-1}	-	mm	d^{-1}	-	mm	d^{-1}
Reference scenario (static)	4	8.20	0.196	4	10.53	0.34	4	11.70	0.423
Dry scenario (static)	8	8.20	0.196	0	-	-	4	11.70	0.423
Wet scenario (static)	4	8.20	0.196	0	-	-	8	11.70	0.423

Table 3: Scenario set up in the "*dynamic*" approach. Duration and Poisson distribution parameters (η and λ) are reported in the dry and wet season.

Dynamic scenario	Dry season			Wet season		
	months	η	λ	months	η	λ
	-	mm	d^{-1}	-	mm	d^{-1}
	random	9.34	0.243	random	11.99	0.413

Table 4: Descriptive statistics of annual water balance components obtained in the three scenarios in the "*static*" approach. Units are mm, except for CV (%).

Scenario	Variable	R	WY	ET_a	GR
		mm	mm	mm	mm
Reference scenario	mean	1229.0	433.3	605.2	194.3
	stand. dev.	176.0	104.2	36.5	48.0
	CV (%)	14.3	24.1	6.0	24.7
	min	586.6	150.8	449.1	44.0
	max	2053.9	1005.9	743.0	389.6
Dry scenario	mean	987.7	317.3	545.1	128.0
	stand. dev.	155.5	88.1	40.8	42.7
	CV (%)	15.7	27.8	7.5	33.4
	min	498.7	96.2	396.0	7.2
	max	1649.9	802.4	691.6	319.3
Wet scenario	mean	1392.8	526.0	625.8	248.1
	stand. dev.	192.4	119.6	34.3	52.6
	CV (%)	13.8	22.7	5.5	21.2
	min	721.9	157.0	481.2	59.0
	max	2179.2	1088.2	748.6	461.6

Table 5: Water balance components associated to occurrence probabilities for each duration of the rainy period.

	Probability	R	WY	ET_a	GR
	%	mm	mm	mm	mm
3-4 months	0.6%	1,145.0	385.3	608.5	169.6
4-5 months	23%	1,213.4	420.0	619.4	188.0
5-6 months	62%	1,275.4	453.0	624.9	199.6
6-7 months	14%	1,326.0	480.2	631.6	210.2
7-8 months	0.3%	1,383.5	511.6	644.2	211.8

Table 6: Exponential regression models, with the corresponding coefficient of determination (R^2), for the wet and dry seasons as a function of the duration of the rainy period.

Duration	Wet season		Dry season	
	Exp regression function	R^2	Exp regression function	R^2
3-4 months	$WY/R = 0.5914 \times \exp(-1.674 \times ET_p/R)$	0.440	$WY/R = 0.4635 \times \exp(-0.343\ ET_p/R)$	0.482
4-5 months	$WY/R = 0.6031 \times \exp(-1.536 \times ET_p/R)$	0.579	$WY/R = 0.3675 \times \exp(-0.204 \times ET_p/R)$	0.290
5-6 months	$WY/R = 0.6171 \times \exp(-1.477 \times ET_p/R)$	0.587	$WY/R = 0.3530 \times \exp(-0.174 \times ET_p/R)$	0.279
6-7 months	$WY/R = 0.6313 \times \exp(-1.399 \times ET_p/R)$	0.617	$WY/R = 0.3476 \times \exp(-0.159 \times ET_p/R)$	0.284
7-8 months	$WY/R = 0.6586 \times \exp(-1.389 \times ET_p/R)$	0.585	$WY/R = 0.3137 \times \exp(-0.105 \times ET_p/R)$	0.211

654

655